J Solid State Electrochem (2008) 12:363–373
DOI 10.1007/s10008-007-0406-1

ORIGINAL PAPER

Effect of FeO_x on the electrocatalytic properties of $NiCo_2O_4$ for O_2 evolution from alkaline solutions

E. Guerrini · M. Piozzini · A. Castelli · A. Colombo · S. Trasatti

Received: 19 December 2006 / Revised: 18 May 2007 / Accepted: 11 June 2007 / Published online: 5 September 2007

Abstract Mixtures of $NiCo_2O_4$ and FeO_x were obtained by thermal decomposition of the nitrates of Ni, Co, and Fe in appropriate proportions. Two series of electrodes were prepared: (1) at constant composition (20 mol% FeO_x) and various calcination temperatures in the range 200 to 480 °C and (2) at constant calcination temperature (300 °C) and various compositions in the whole composition range 0 to 100 mol% FeO_x. The oxide layers were characterized by thermogravimetric analysis, X-ray diffraction, scanning electron microscopy, and cyclic voltammetry. Experimental data showed that the layers consist of a mixture of phases in which Fe oxide is present as Fe_2O_3. The electrocatalytic properties were assessed by means of quasi-stationary potentiostatic current-potential curves for the O_2 evolution reaction from alkaline solution. Results have shown that the mechanism of O_2 evolution depends on composition moderately. The electrocatalytic activity appears to depend on composition only slightly.

Keywords Electrocatalysis · O_2 evolution · Oxide electrodes · $NiCo_2O_4$ · Fe oxide

Dedicated to Professor Oleg Petrii on the occasion of his 70th birthday on August 24th, 2007.

E. Guerrini · M. Piozzini · A. Castelli · A. Colombo · S. Trasatti (✉)
Department of Physical Chemistry and Electrochemistry,
University of Milan,
Via Venezian 21,
20133 Milan, Italy
e-mail: sergio.trasatti@unimi.it

Introduction

O_2 evolution is a very "demanding" reaction [1, 2], thus, bearing adversely on the economy of electrochemical processes, in particular water electrolysis that is traditionally carried out in alkaline solution [3]. For this reason, extensive search for new electrode materials with better electrocatalytic properties has been carried out for several decades.

This paper is dedicated to O.A. Petrii who has worked in the field of electrocatalysis for more than 40 years, contributing not only experimentally but also theoretically to our understanding of this fundamental area of electrochemistry [4–8].

Ni has long been used as an anode for technological applications in strongly alkaline solution [9]. Although this metal possesses a relatively low overpotential for O_2 evolution [10, 11], it is appreciably unstable under prolonged anodic polarization, especially under conditions of intermittent electrolysis of interest for on-site water electrolyzers powered by photovoltaic devices for direct solar energy conversion [12–14].

Activation and stabilization of Ni electrodes are achieved by depositing thin films of oxide electrocatalysts, e.g., NiO_x [15], Co_3O_4 [16] or, better still, $NiCo_2O_4$ [17, 18] by thermal decomposition of suitable precursors. It has been occasionally observed [19] that impurities of Fe coming from the corrosion of the case of power sources decrease dramatically the O_2 overpotential of both Ni and Co oxides.

In a previous work [20], we investigated the electrocatalytic properties of mixtures of NiO_x + FeO_x. It was found that FeO_x reduces the overpotential of NiO_x for O_2 evolution while increasing its stability. Activation was observed in the composition range 10 to 60% FeO_x, although *true* electrocatalytic effects go through a sharp maximum at ca 10–20% FeO_x.

In the present work, the study of the effect of FeO_x has been extended to $NiCo_2O_4$, known as one of the best electrocatalyst for O_2 evolution in alkaline solution.

Experimental

Supports

Supports were Ni platelets of 10×10×0.2 mm with a stem of 2×50 mm attached to one of the sides in central position. Supports were sandblasted with quartz powder and ultrasonicated before the deposition of the precursor. The special holder for electrodes has been described previously [21].

Electrodes

$Ni(NO_3)_2{\cdot}6H_2O$, $Co(NO_3)_2{\cdot}6H_2O$, and $Fe(NO_3)_3{\cdot}9H_2O$ were used as precursors. They were dissolved in water in the desired proportions so as to have a total concentration of ca 0.2 mol dm^{-3}. The solution was deposited onto both sides of the support by brushing, the solvent evaporated at <60 °C, and the samples fired in a pre-heated oven for 5 min. The operation was repeated until the amount deposited was about 1 mg cm^{-2}.

Two series of electrodes were prepared. In a first series, electrodes of composition 20 mol% FeO_x + 80 mol% $NiCo_2O_4$ were fired at 15 different temperatures between 200 and 480 °C at 20 °C intervals. Three specimens were prepared at each temperature, two for electrochemical experiments and one for physico-chemical characterizations.

In a second series, electrodes were prepared at 300 °C in ten different compositions between 0 and 100 mol% FeO_x in 10 ml% steps (except 90 mol%), three specimens at each composition. In total, 45 samples at different temperatures and 30 samples at different compositions.

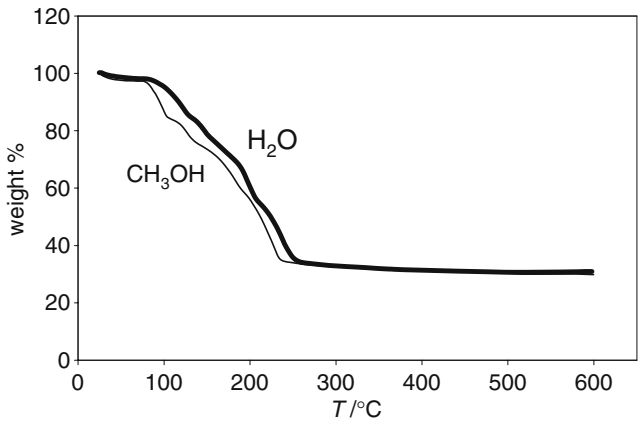

Fig. 1 Thermogravimetric curve of a mixture of Co, Ni, and Fe nitrates with 20 mol% Fe. Precursors were first dissolved into the solvents indicated. Scan rate, 10 °C/min

Solutions

KOH solutions (1 mol dm^{-3}) were used for all electrochemical measurements. All experiments were carried out at 25±0.1 °C in a water thermostat. Solutions were deaerated by bubbling purified N_2, which also provided some stirring during the experiments.

Reference electrode

Unless otherwise stated, a saturated calomel electrode was used as a reference electrode. Electrode potentials are reported on the (SCE) scale.

Methods

Pysico-chemical characterization was carried out by means of thermogravitric analysis (TGA), X-ray diffraction (XRD), and scanning electron microscopy (SEM). XRD was used for the series at different composition only, whereas SEM pictures were taken for selected samples of both series.

Electrochemical studies were carried out using a 273A model EG&G potentiostat-galvanostat driven by a PC using the M270 software.

The surface electrochemical response of the electrodes was studied by cyclic voltammetry at 20 mV/s. The explored potential range was 0 to 0.5 V (SCE), the anodic limit being just before O_2 evolution. The surface charge was obtained by integration of the voltammetric curves using the same software.

The kinetics of O_2 evolution was studied by quasi-stationary current-potential curves. Anodic polarization curves were recorded point by point in 10 mV steps. The current was read after 1 min at each potential. Readings were normally limited to about 0.1 A cm^{-2}. Unless otherwise stated, current densities are reported on the basis of the apparent surface area.

Results and discussion

Thermogravimetry

Figure 1 shows the TGA curve of 80 mol% $NiCo_2O_4$ + 20 mol% FeO_x recorded at a scan rate of 10 °C/min. The precursor was dissolved in two different solvents and the latter evaporated at 60 °C. The curves are qualitatively similar, with that for H_2O shifted by ca 20 °C to higher temperatures. In view of this outcome, H_2O was chosen as a solvent for all experiments.

Figure 1 shows that decomposition starts close to 100 °C and ends close to 250 °C. Decomposition appears to take

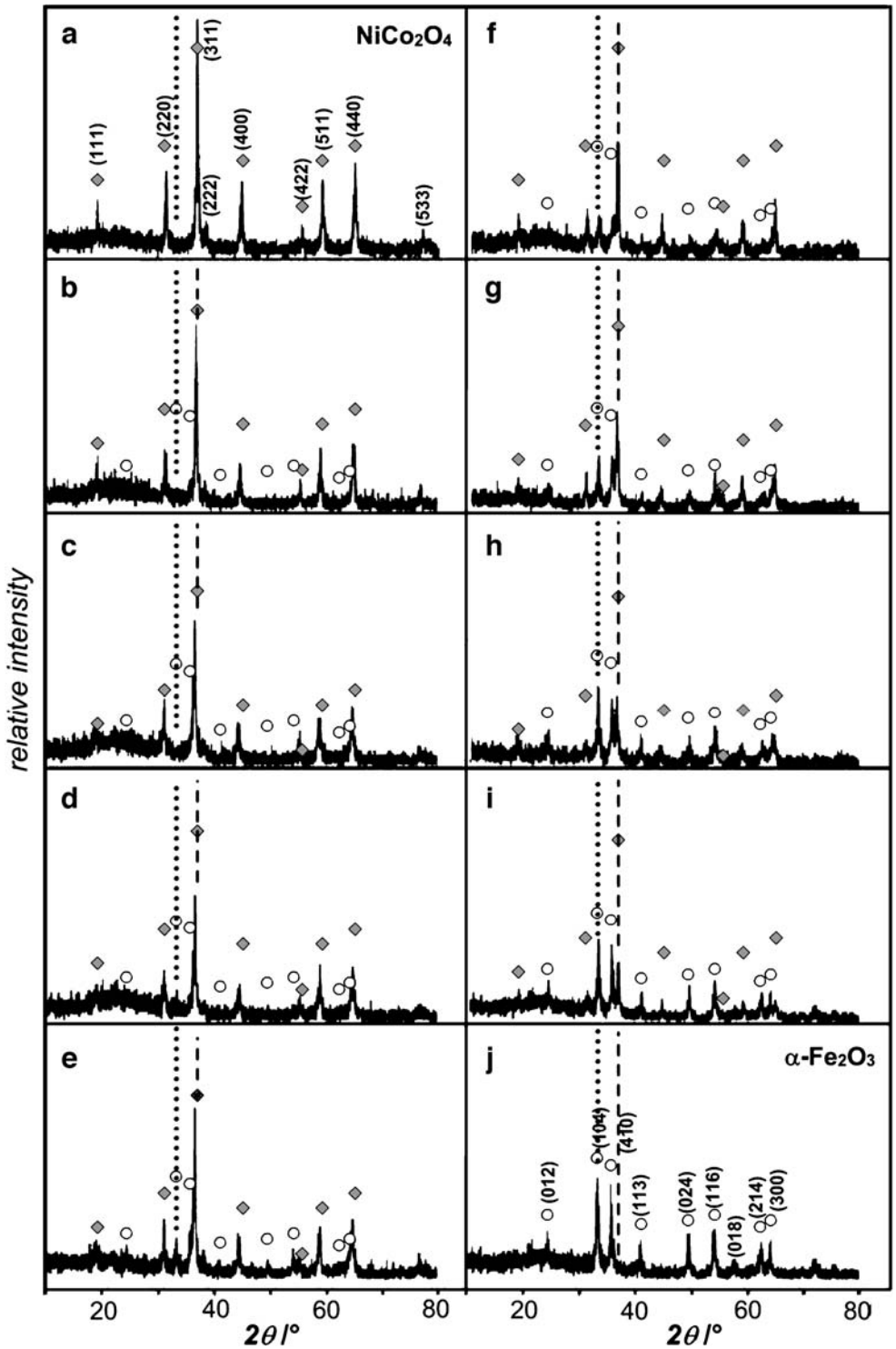

Fig. 2 XRD spectra of $NiCo_2O_4$ + *n* mol% FeO_x mixtures of various compositions. Calcination temperature: 300 °C. *n* = **a** 0, **b** 10, **c** 20, **d** 30, **e** 40, **f** 50, **g** 60, **h** 70, **i** 80, **j** 100. (*filled diamond*) $NiCo_2O_4$; (*open circle*) Fe_2O_3

place in several steps presumably related to the strong hydration of the precursors. The overlapping of the curves at $T>250$ °C suggests that the final products are compositionally the same irrespective of the solvent of the precursors.

Since with $(dT/dt)\neq 0$ TGA curves are shifted to higher temperatures, 300 °C was chosen as the lowest realistic temperature for complete decomposition. Thus, mixed oxides of $NiCo_2O_4$ and FeO_x were prepared at such temperature.

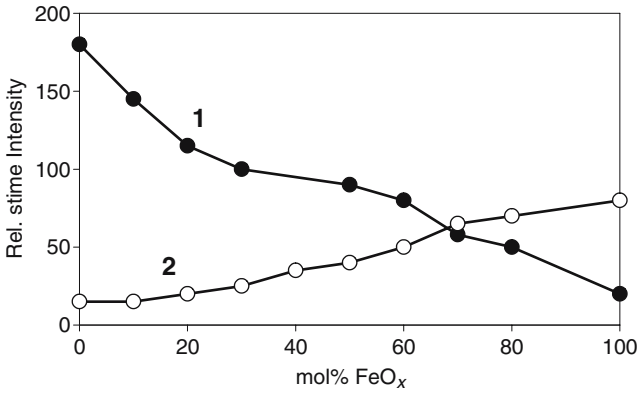

Fig. 3 Variation with composition of two main peaks for (1) $NiCO_2O_4$ (ca 37°) and (2) Fe_2O_3 (ca 33°)

XRD analysis

Figure 2 gives an exhaustive view of XRD spectra for samples prepared at 300 °C at all compositions from 0 to 100% FeO_x. Comparison with reference standards revealed that both samples at 0 and 100% FeO_x consist of a single phase, $NiCo_2O_4$ and Fe_2O_3, respectively. For the pure components, the main peaks are identified and the crystal orientation indicated. At intermediate compositions, the spectra appear to result from the superposition of those of the two components. In other words, the solid consists of a mixture of phases. This is made evident by the dashed line drawn vertically at the position of the main peak for each of the pure components. No shift is visible as the composition is changed. This is further proven by Fig. 3 where the intensity of the main peaks (at ca 37° for $NiCo_2O_4$ and ca 33° for Fe_2O_3) are plotted as a function of the nominal composition. The variation is monotonic for both phases. The non-zero intensity of the signals pertaining to the absent components is due to the fact that the spectra include the background. As intensities are on a relative scale, the picture of the situation is not distorted.

SEM micrographs. Morphology of oxide layers

Layers look rough but homogeneous. Figure 4 shows the effect of temperature at constant composition (20% FeO_x). At 200 °C, the layer looks clearly amorphous, being mostly the solid precursor still incompletely decomposed. At higher temperatures, decomposition results in the formation of globules whose size increases as T is increased.

Although the apparent height of asperities might suggest that if in some places it is higher than the average film thickness some fragments of the support might remain uncovered, this is very unlikely to be the case if it is considered that the support is very rough, and the apparently variable thickness of the overlayer largely reflects the underlying roughness.

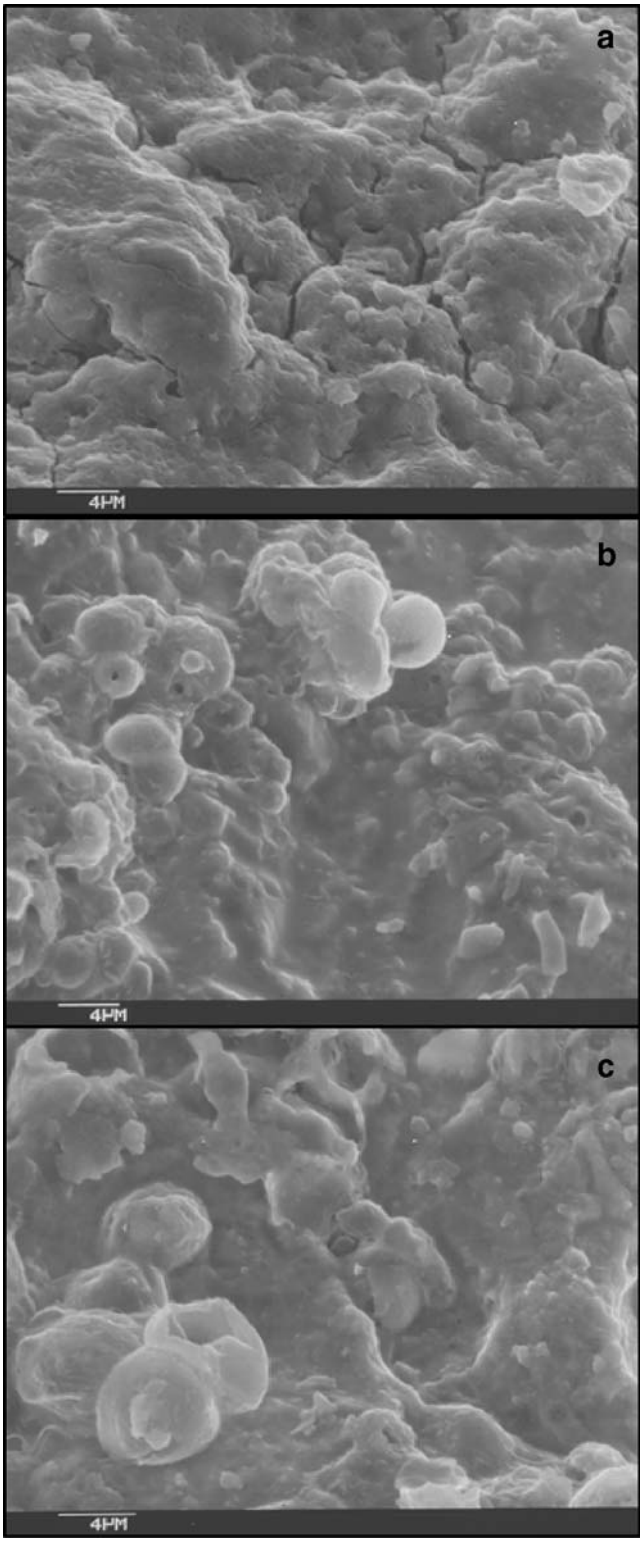

Fig. 4 SEM micrographs (5,000×) of $NiCo_2O_4$ + 20 mol% FeO_x calcined at **a** 200 °C, **b** 300 °C, **c** 480 °C

Figure 5 shows the effect of composition at constant temperature of calcination (300 °C). The main feature is the decrease of the volume of the globules with increasing FeO_x content up to complete disappearance already at 70%

FeO_x. This indicates prevalence of finer particles in FeO_x-rich samples. Although not straightforwardly related to particle size, the relative intensity of the main XRD peaks is noted to be appreciably lower for pure FeO_x than for pure $NiCo_2O_4$.

Voltammetric curves

Voltammetric curves can be regarded as electrochemical spectra. They constitute the electrochemical fingerprint of a given compound and can give information on surface morphology [22]. As argued in the previous paragraph, the support is very unlikely to contribute to define the shape of the voltammetric curves.

Figure 6 shows the effect of temperature at constant composition (20% FeO_x). The curves exhibit two peaks, one on the anodic side close to 0.4 V (SCE) the other on the cathodic side close to 0.2 V. The pattern is typical of $NiCo_2O_4$ [23, 24] that evidently prevails upon that of Fe_2O_3. As the temperature of calcination is increased, the peaks become closer and less distorted. This is typical of increasing crystallinity with increasing temperature, in agreement with XRD and SEM data. For the sample calcined at 200 °C, the higher current range indicates a more extended surface area, in accord with the presence of finer particles as mentioned above (see next paragraph).

Figure 7 shows the effect of composition at constant temperature of calcination. As the content of FeO_x increases, the height of the peaks decreases to give a featureless curve at 100% FeO_x. This is a consequence of the fact that Fe(III) does not undergo further anodic oxidation, and therefore, no related reduction peak appears cathodically [20]. In addition, Fe_2O_3 is more resistive than $NiCo_2O_4$, and this contributes to distort the voltammetric curve with increasing separation of eventual redox peaks.

Voltammetric charge

Integration of voltammetric curves gives the voltammetric charge, q^*, related to surface redox transitions. As the latter involve the exchange of protons with the solution [22]:

$$MO_x(OH)_y + \delta H^+ + \delta e \rightarrow MO_{x-\delta}(OH)_{y+\delta} \quad (1)$$

q^* can be assumed to measure the surface concentration of active sites, i.e., sites exchanging protons with the solution.

Figure 8a shows the dependence of q^* on calcination temperature at constant composition (20% FeO_x) for fresh electrodes. There are three characteristic features:

1) Up to ca 300 °C q^* decreases with increasing T. This is due to increasing crystallization and sintering with consequent decrease in surface area.

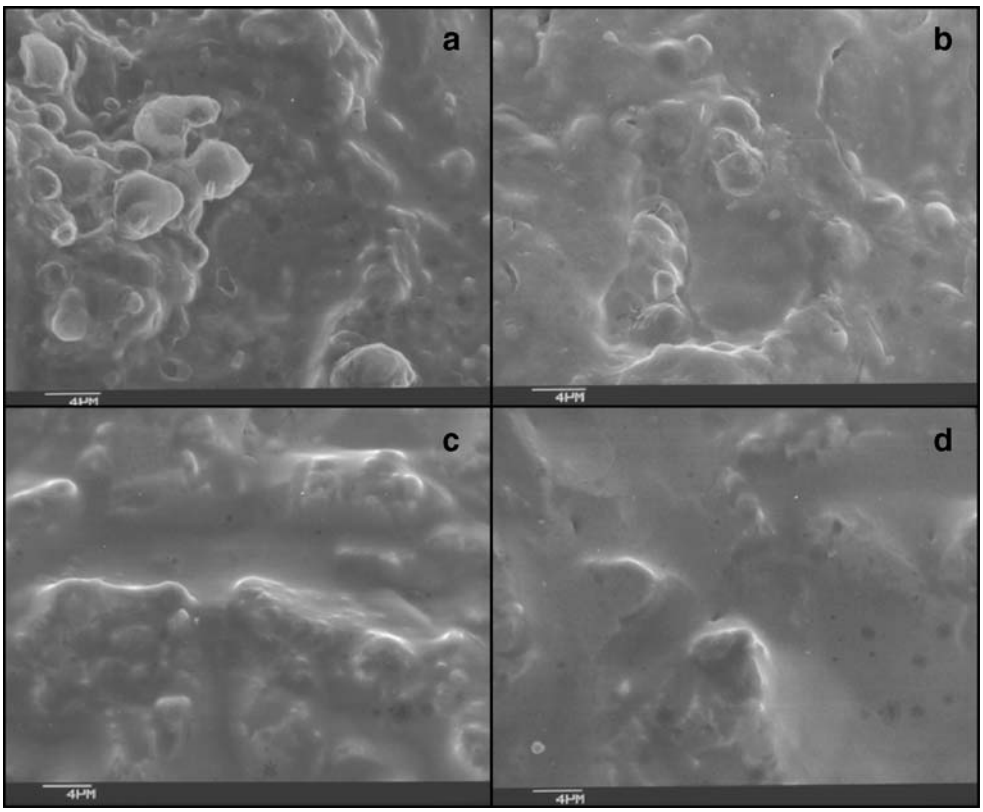

Fig. 5 SEM micrographs (5,000×) of $NiCo_2O_4$ + n mol% FeO_x calcined at 300 °C. n = **a** 0, **b** 30, **c** 50, **d** 70

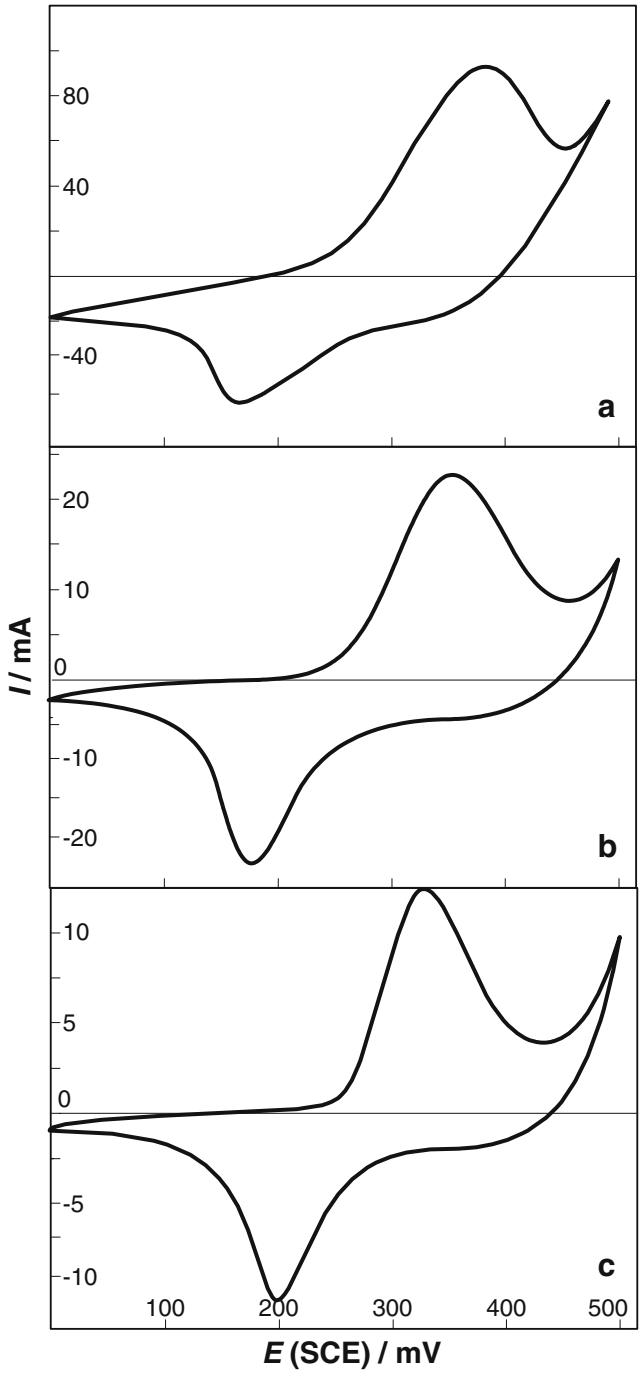

Fig. 6 Cyclic voltammetric curves of $NiCo_2O_4$ + 20 mol% FeO_x electrodes prepared at different temperatures. **a** 200, **b** 300, **c** 400 °C

2) Close to 330 °C, there appears a hump. This is not an experimental artifact, as it proved reproducible. As no weight loss is associated (cf. Fig. 1), it can be interpreted as a phase transition or recrystallization.
3) At T>450 °C, q^* appears to increase again. This is also reproducible and can be explained in terms of spinel thermal decomposition, as experimentally known [25]. Decomposition as a rule results in surface area increase.

Figure 8b shows the dependence of q^* on composition at constant calcination temperature (300 °C). The voltammetric charge remains almost constant up to ca 60% FeO_x, then it drops to very low values. The sharp decrease can be associated with the absence of redox transitions on the surface of Fe_2O_3. Thus, up to ca 60% FeO_x, the surface behavior is essentially governed by $NiCo_2O_4$, while for >60% FeO_x the latter prevails. The non-linear dependence of q^* on nominal composition for <60% FeO_x points to some surface enrichment phenomena of $NiCo_2O_4$ at the surface of the active layer.

Tafel lines

Figure 9 shows a typical polarization curve for O_2 evolution. No detectable hysteresis is observed between forward and backward polarization scan. A linear region (Tafel region) is easily visible in the 0.4- to 0.5-V potential range. Deviations at more anodic potentials can be due either to uncompensated ohmic drops or to a second Tafel line + IR drops.

To distinguish between the two possibilities, two approaches are possible:

1) ΔE values are calculated in the deviation potential range between the experimental points and the straight line drawn through the points. The ΔE values are then plotted against the corresponding current (Fig. 10a). A straight line would indicate that deviations are due to ohmic drops and that only one Tafel line exists.
2) As in the presence of ohmic drops a Tafel line can be written:

$$E = a + b \ln I + RI \tag{2}$$

it results:

$$\left(\frac{dE}{dI}\right) = \frac{b}{I} + R \tag{3}$$

A plot of $(\Delta E/\Delta I)$ vs $(1/I)$ is shown in Fig. 10b. A single straight line is observed, whose slope gives b and whose intercept gives R. This plot confirms the existence of a single Tafel slope, i.e., the mechanism of O_2 evolution on a given electrode does not change with the potential range.

Tafel slope

Tafel slopes obtained using the two approaches described above were found in substantial agreement. Figure 11a shows the dependence of b on calcination temperature. A considerable scattering is actually observed. Nevertheless, a trend appears clearly: The Tafel slope is low around 40 mV up to 300–350 °C; then, it increases to around 60 mV. It is

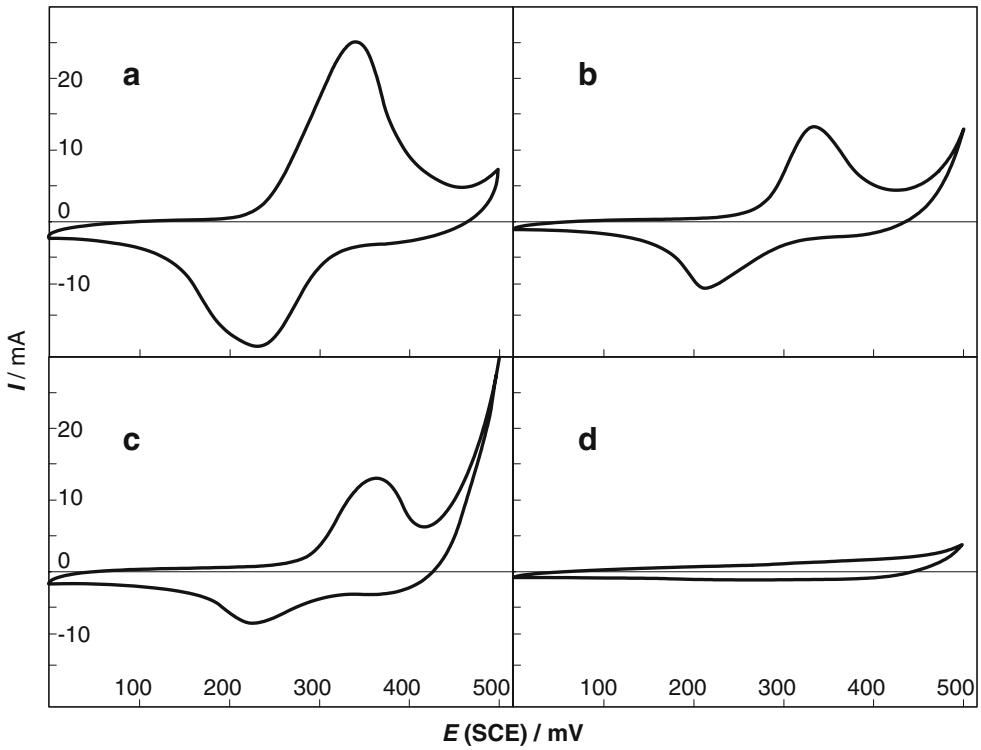

Fig. 7 Cyclic voltammetric curves of $NiCo_2O_4$ + *n* mol% FeO_x calcined at 300 °C. *n* = **a** 0, **b** 40, **c** 60, **d** 80

intriguing that the transition temperature is in the same range as in Fig. 8. This indicates that the apparent phase transition affects the properties of the surface.

Figure 11b shows the dependence of *b* on composition. In this case, the Tafel slope decreases from 60 mV to around 40 mV, as only 10 mol% FeO_x is added to $NiCo_2O_4$ and does not change very much for further addition of FeO_x, although there is a hint to increase as the FeO_x content exceeds 60%. It is also intriguing that this composition does not differ from that in Fig. 8b. A sharp effect of the addition of FeO_x was also observed previously [20] for mixtures with NiO_x.

As a matter of fact, the Tafel slope for O_2 evolution varies between 40 and 60 mV depending on calcination temperature and FeO_x content. In other words, the reaction mechanism is slightly dependent on these two variables.

Uncompensated ohmic drop

Figure 12 shows the dependence of *R* on (a) calcination temperature and (b) FeO_x content. The plots are self-evident and do not require much explanation. *R* can be attributed to the resistance between the electrode surface and the tip of the Luggin capillary. An average value close to 0.5 ohm is typical of solution resistance. As *R* exceeds such value, the excess is to be attributed to the oxide film. Thus, Fig. 12b shows that an increasing content of FeO_x contributes to *R* sizably. As the calcination temperature increases, *R* rises presumably because of collapse of the lattice of $NiCo_2O_4$.

The increasing value of *R* as the FeO_x content increases might suggest that the disappearance of the peaks in Fig. 7d could be related to a pronounced shift of the peaks. However, this is unlikely for two reasons: (1) The value of *R* for 80% FeO_x is not typical of an insulating oxide such as TiO_2 or Ta_2O_5. In other words, the ohmic drop is not so high as to justify a peak shift of more than 200 mV; (2) the potential scan rate in Fig. 7 is only 20 mV/s, relatively low to give such high peak shifts with a relatively small ohmic resistance.

Reaction mechanism

On the basis of Tafel slopes, it is possible to put forward a plausible mechanism for the O_2 evolution reaction. The Tafel slope of 40 mV points to a second electron transfer as the rds, while 60 mV indicate a chemical step after the primary discharge. A general mechanism thus conforms to the scheme previously proposed by one of us [1]:

$$S + OH^- \rightarrow S - OH* + e \quad (4a)$$

$$S - OH* \rightarrow S - OH \quad (4b)$$

$$S - OH + OH^- \rightarrow S - O + H_2O + e \quad (4c)$$

$$2S - O \rightarrow 2S + O_2 \quad (4d)$$

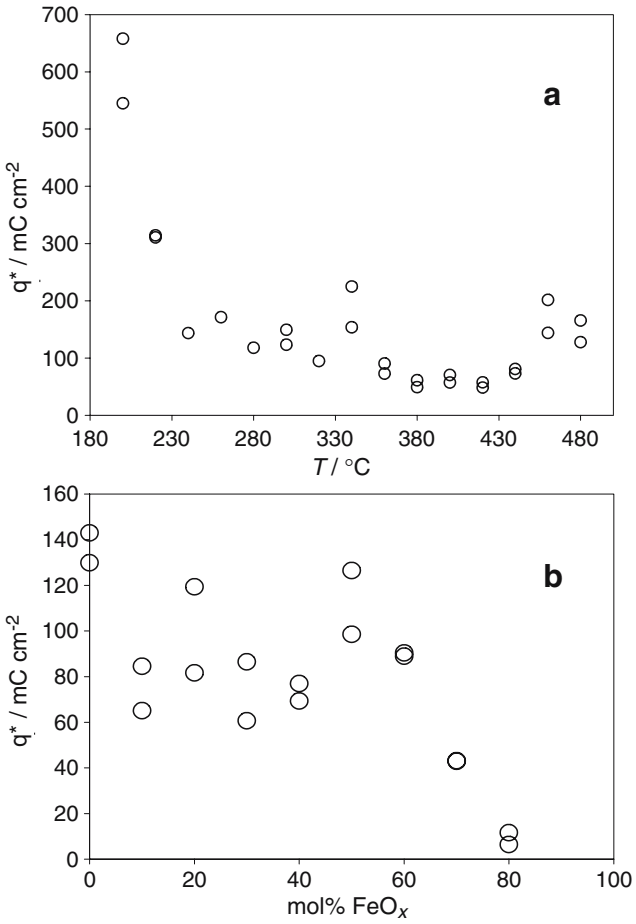

Fig. 8 **a** Voltammetric charge (q^*) by integration of curves in Fig. 6 as a function of calcination temperature. **b** Voltammetric charge (q^*) by integration of curves in Fig. 7 as a function of composition

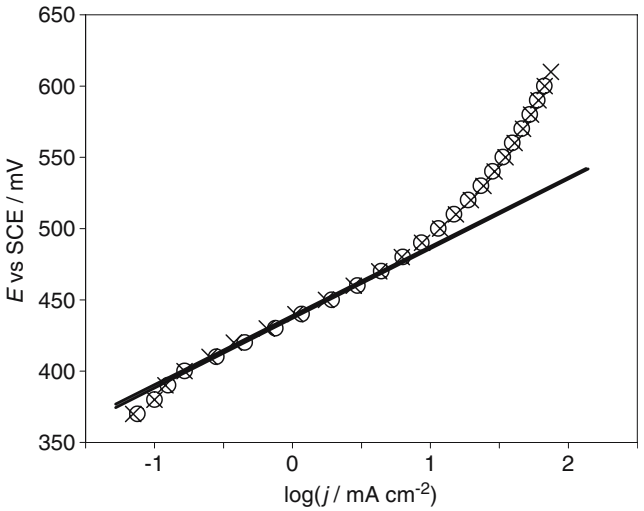

Fig. 9 Typical polarization curve for O_2 evolution from 1 mol dm^{-3} KOH solution. (*open circle*) Forward and (*x*) backward polarization data are shown. The apparent Tafel line has been drawn through the points

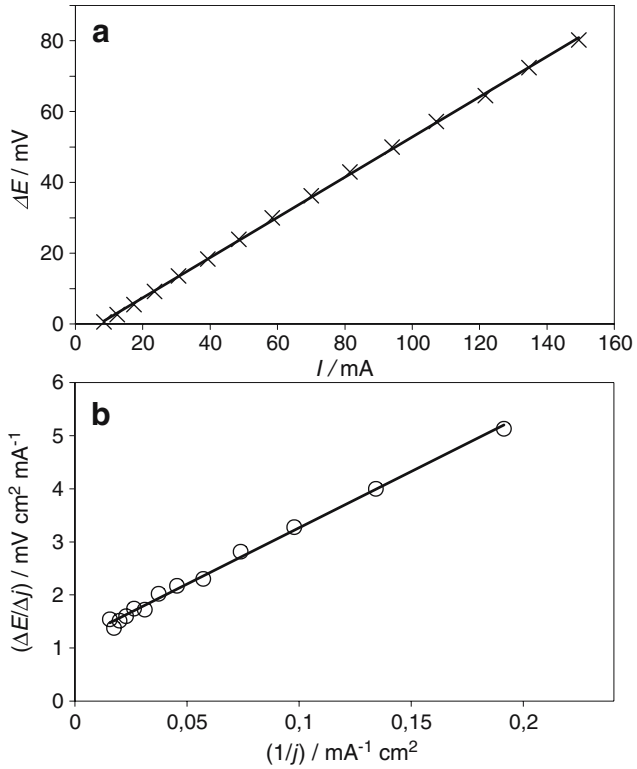

Fig. 10 **a** ΔE vs I from the plot in Fig. 9. **b** ($\Delta E/\Delta j$) vs ($1/j$) from the experimental data of Fig. 9

S is a surface active site. Step (4a) is the primary discharge. S–OH* is an unstable surface intermediate that can evolve to a more stable S–OH (spillover). Step (4c) is the second electron transfer. Thus, with b=40 mV, step (4b) is fast and step (4c) is rate-determining. This analysis requires that the coverage with intermediates is low ($\vartheta_{OH} \approx 0$). With b=60 mV, step (4b) becomes rate-determining. The discriminant between the two mechanisms is thus the strength of interaction of the intermediates with the electrode surface, which implies increase in the adsorption strength of the intermediates from pure $NiCo_2O_4$ to mixtures with FeO_x. This is in line with concepts of electrocatalysis for oxide electrodes [26, 27].

Structure–activity relations

Figure 13 shows the correlation between current density (activity) at E=0.48 V (SCE) of electrodes calcined at different temperatures and the corresponding voltammetric charge, q^*, measured at the end of the experiment of O_2 evolution. The dependence is non-linear, and the increase is more than proportional with increasing q^*. This indicates that electronic effects are operating besides geometric effects. More specifically, the over-proportionality is taken to imply a particle size effect, since as q^* increases, particles become smaller.

A correlation between j and q^* for electrodes at different composition is not straightforwardly significant considering that FeO_x does not contribute to q^*, although it evolves O_2. However, if j at 0.48 V is plotted against composition, Fig. 14a shows a pattern similar to that of q^* vs composition. In other words, the electrocatalytic effect of FeO_x added to $NiCo_2O_4$ appears of moderate importance.

Allowance for geometric factors can be attempted by normalizing j to unit surface charge. Figure 14b shows a plot of (j/q^*) vs composition. Apparently, the normalized activity increases with the content of FeO_x, but such a plot is affected by the fact that FeO_x does not contribute to q^*, and therefore, (j/q^*) increases as an artifact as the Fe_2O_3 content increases.

Stability

As q^* measures the surface morphology of the electrodes, comparison of q^* for the same electrode before and after a given experiment can provide some indication about whether the surface state has been affected.

Figure 15 shows correlations of q^* for fresh samples vs q^* after O_2 evolution experiments for electrodes at constant composition (20% FeO_x) and variable calcination temperature (a), as well as for electrodes at constant calcination temperature (300 °C) and variable composition (b). In both cases, O_2 evolution causes decrease in q^*. For samples at constant composition, the decrease is roughly proportional to q^* and amounts to about 20%. This suggests that the calcination temperature is not a crucial factor for stability. The decrease of q^* can thus be attributed to mechanical erosion of loosely held particles.

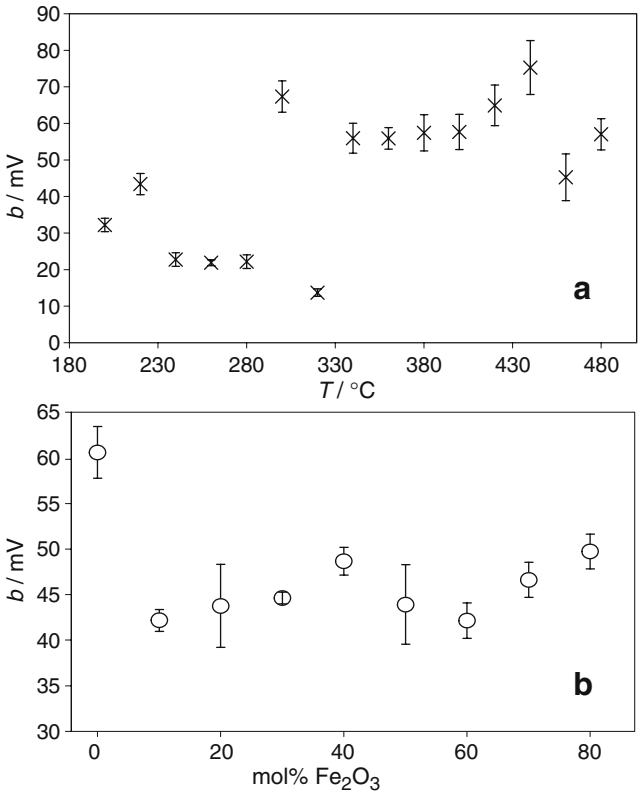

Fig. 11 **a** Tafel slope for O_2 evolution on $NiCo_2O_4$ + 20 mol% FeO_x as a function of calcination temperature. **b** Tafel slope for O_2 evolution on $NiCo_2O_4$ + n mol% FeO_x as a function of composition

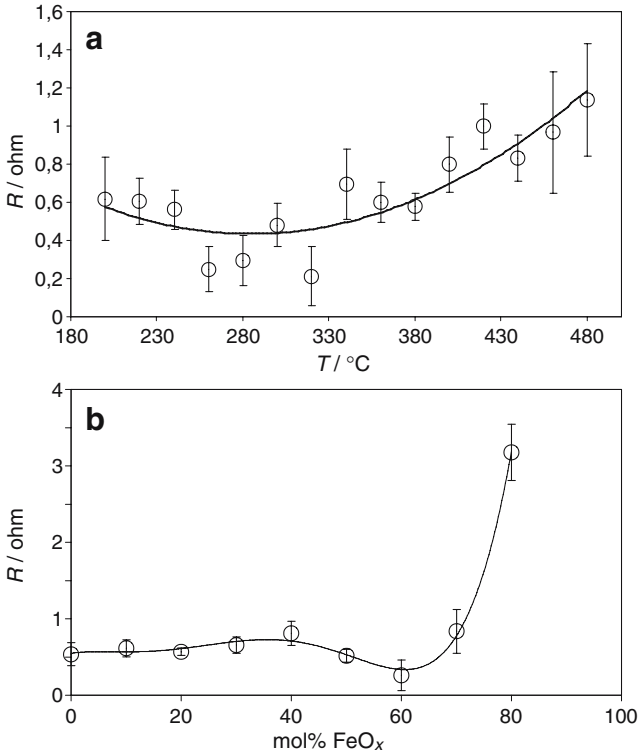

Fig. 12 **a** Uncompensated ohmic resistance as a function of the calcination temperature for $NiCo_2O_4$ + 20 mol% FeO_x electrodes. **b** Uncompensated ohmic resistance as a function of composition for $NiCo_2O_4$ + n mol% FeO_x calcined at 300 °C

For samples at different compositions, interpretation is more difficult, as FeO_x does not contribute appreciably to q^*, but q^* is not linearly dependent on mol% FeO_x. Thus, a higher value of q^* cannot straightforwardly be associated with a higher content of FeO_x. Nevertheless, as q^* is low at high content of FeO_x>60 mol%, Fig. 15b could be tentatively interpreted as indicating higher stability for higher FeO_x contents. This conclusion can be corroborated by the inset of Fig. 15b where the ratio (q^*_a/q^*_b; a = after, b = before) is reported singularly for each electrode as a function of the content of FeO_x.

Conclusions

– Iron oxide is present as Fe_2O_3 in mixed oxides with $NiCo_2O_4$.

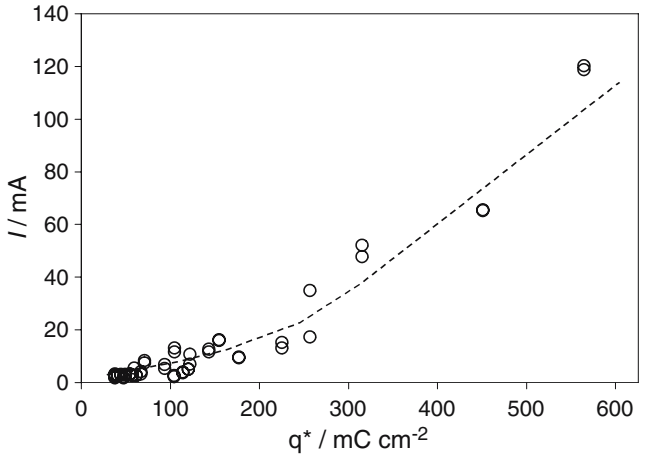

Fig. 13 Current of O_2 evolution at E=0.48 V(SCE) as a function of the pertinent voltammetric charge (q*)

– The structure of the mixed oxides corresponds to a phase mixture, as the characteristic peaks of XRD for the separate phases can be distinguished at every composition.

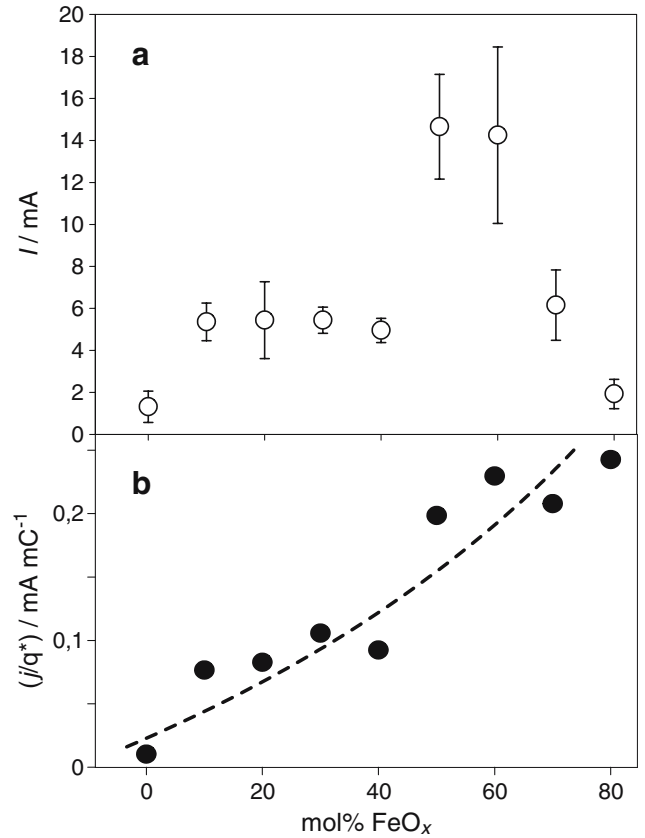

Fig. 14 **a** Current of O_2 evolution at E=0.48 V(SCE) as a function of electrode composition. **b** Current of O_2 evolution normalized to unit voltammetric charge as a function of electrode composition

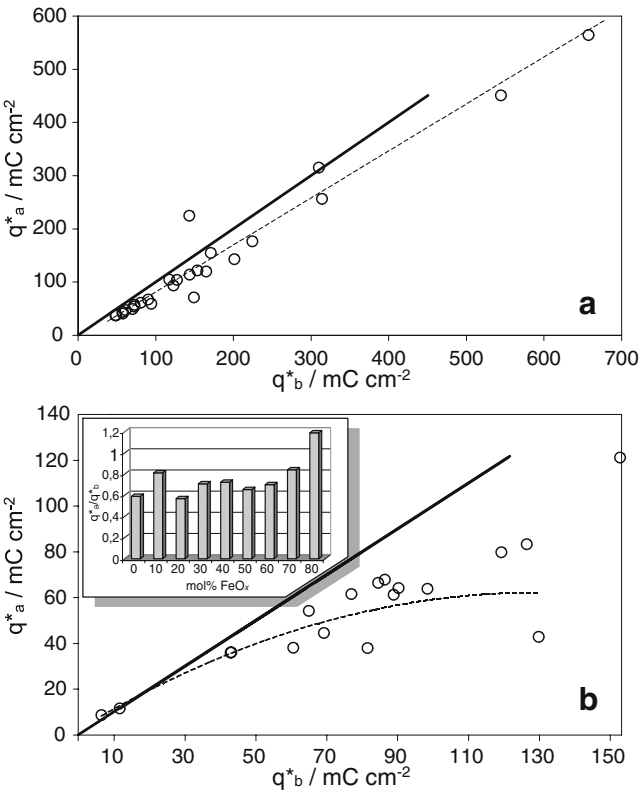

Fig. 15 **a** Plot of voltammetric charge (q*) after O_2 evolution experiments against q* for fresh electrodes calcined at various temperatures. **b** Plot of voltammetric charge (q*) after O_2 evolution experiments against q* for fresh electrodes of various compositions. *Inset:* ratio of q* after vs before O_2 evolution as a function of electrode composition

– The morphology of the layers depends on composition: more crystalline at the $NiCo_2O_4$ end, more amorphous at the Fe_2O_3 end.
– The voltammetric charge indicates that there is surface enrichment with $NiCo_2O_4$ for FeO_x<60%, and FeO_x enrichment for FeO_x>60%.
– The mechanism of O_2 evolution appears to change both with calcination temperature and composition. The Tafel slope varies between 40 and 60 mV. The corresponding mechanism is ECE where the rds moves from the second E to C. The chemical step is proposed to be spillover of oxygenated intermediates. The change in mechanism is related to the bond strength of intermediates to surface active sites.
– FeO_x contributes moderately to the electrocatalytic activity of oxide mixtures that is essentially determined by the properties of $NiCo_2O_4$. As FeO_x activates NiO [20], it is to be concluded that the combination of Ni with Co produces more important synergic effects.
– FeO_x contributes to the stability of mixed oxides, although its actual effect is difficult to disentangle from other contributions.

References

1. Trasatti S (1990) Electrode kinetics and electrocatalysis of hydrogen and oxygen electrode reactions. 4. The oxygen evolution reaction. In: Wendt H (ed) Electrochemical hydrogen technologies. Elsevier, Amsterdam, pp 104–135
2. Trasatti S, Lodi G (1981) Oxygen and chlorine evolution at conductive metallic oxide anodes. In: Trasatti S (ed) Electrodes of conductive metallic oxide, Part B. Elsevier, Amsterdam, pp 521–626
3. Pletcher D, Walsh FC (1990) Industrial electrochemistry, 2nd edn. Chapman & Hall, London, p 260
4. Nikiforova TG, Petrii OA (2005) Russ J Electrochem 41:118
5. Petrii OA, Tsirlina GA (2001) Usp Khim 70:330
6. Pron'kin SN, Tsirlina GA, Petrii OA, Vassiliev SY (2001) Electrochim Acta 46:2343
7. Petrii OA, Safonova TY, Tsirlina GA, Rusanova MY (2000) Electrochim Acta 45:4117
8. Petrii OA, Kalinin VD (1999) Russ J Electrochem 35:627
9. Wendt H, Plzak V (1990) Electrocatalysis and electrocatalysts for cathodic evolution and anodic oxidation of hydrogen. In: Wendt H (ed) Electrochemical hydrogen technologies. Elsevier, Amsterdam, pp 15–62
10. Trasatti S (1992) Electrocatalysis of hydrogen evolution: progress in cathode activation. In: Gerischer H, Tobias CW (eds) Advances in electrochemical science and engineering. VCH, Weinheim, pp 1–85
11. Mahmmood MN, Turner AK, Man MCM, Fogarty PO (1984) Chem Ind 50
12. Trasatti S (1995) Int J Hydrogen Energy 20:835
13. Divisek J, Mergel J, Schmitz H (1990) Int J Hydrogen Energy 15:105
14. Ahmad GE, El Shenawy ET (2006) Renew Energy 31:1043
15. Miller EL, Rocheleau RE (1997) J Electrochem Soc 144:1995
16. El Baydi M, Poillerat G, Rehspringer J-L, Gautier JL, Koenig J-F, Chartier P (1994) J Solid State Chem 109:281
17. Yang J, Li JB, Lin H, Yang XZ, Tong XG, Guo GF (2006) J Appl Electrochem 36:945
18. Miller EL, Rocheleau RE (1997) J Electrochem Soc 144:3072
19. Cordoba SI, Carbonio RE, Lopez Teijelo, Macagno VA (1987) Electrochim Acta 32:749
20. Krstajić N, Trasatti S (1996) Surface and electrocatalytic properties of NiO_x + FeO_x mixed oxide electrodes for O_2 evolution. In: Adzic RR, Anson FC, Kinoshita K (eds) Oxygen electrochemistry, vol 95-26. The Electrochemical Society, Pennington, pp 155–165
21. Garavaglia R, Mari CM, Trasatti S (1984) Surf Technol 23:41
22. Trasatti S (1999) Interfacial electrochemistry of conductive oxides for electrocatalysis. In: Wieckowski A (ed) Interfacial electrochemistry: theory, practice, applications. Marcel Dekker, New York, pp 769–792
23. Chi B, Li JB, Han YS, Chen YJ (2004) Int J Hydrogen Energy 29:605
24. Serebrennikova I, Birss VI (2000) J Electrochem Soc 147:3614
25. Roginskaya YuE, Morozova OV, Lubnin EN, Uilitina YuE, Lopukhova GV, Trasatti S (1977) Langmuir 13:4621
26. Trasatti S (1980) J Electroanal Chem 111:125
27. Trasatti S (1994) Transition metal oxides. Versatile materials for electrocatalysis. In: Lipkowski J, Ross PN (eds) The electrochemistry of novel materials. VCH Publishers Inc, New York, pp 207–295